ISSN 0036-0236, Russian Journal of Inorganic Chemistry, 2016, Vol. 61, No. 7, pp. 805–810. © Pleiades Publishing, Ltd., 2016.
Original Russian Text © N.P. Simonenko, E.P. Simonenko, V.G. Sevastyanov, N.T. Kuznetsov, 2016, published in Zhurnal Neorganicheskoi Khimii, 2016, Vol. 61, No. 7, pp. 843–849.

SYNTHESIS AND PROPERTIES OF INORGANIC COMPOUNDS

Preparation of Nanostructured Thin Films of Yttrium Iron Garnet ($Y_3Fe_5O_{12}$) by Sol–Gel Technology

N. P. Simonenko, E. P. Simonenko, V. G. Sevastyanov, and N. T. Kuznetsov

Kurnakov Institute of General and Inorganic Chemistry, Russian Academy of Sciences, Leninskii pr. 31, Moscow, 119991 Russia
e-mail: n_simonenko@mail.ru

Received December 1, 2015

Abstract—The synthesis of hydrolytically active heteroligand coordination compounds $[M(C_5H_7O_2)_{3-x}(C_5H_{11}O^i)_x]$ ($M = Fe^{3+}$ and Y^{3+}) using iron and yttrium acetylacetonates has been studied. The gel formation kinetics in solutions of these compounds upon hydrolysis and polycondensation has also been studied. Thin films of a solution of these precursors have been applied to polished sapphire substrates by dip coating technology. The crystallization of nanostructured yttrium iron garnet ($Y_3Fe_5O_{12}$) films during heat treatment of xerogel coatings under various conditions has been studied. How the phase composition, microstructure, and particle size depend on the synthesis parameters has been recognized.

DOI: 10.1134/S0036023616070184

Everyone knows that yttrium iron garnet is in great demand in the optoelectronic industry thanks to its properties such as low dielectric losses and a narrow width of the ferromagnetic absorption line in the X-band range. This complex oxide is often required in thin films for improving the efficiency of devices. As a rule, physical sputtering methods are used to manufacture coatings, namely, magnetron sputtering [1, 2] or pulsed laser deposition [3–7]. In some cases, doping with rare-earth and other elements, specifically with bismuth, can improve the parameters of $Y_3Fe_5O_{12}$ films [8–10] to make them usable in the design of high-quality magnetic insulators, which have recently become of special interest in the context of spintronic applications. This will fill-in the gap between the technologies of spintronic materials and thermoelectric materials and will provide new opportunities for energy conversion from heat to electricity. In spite of the merits of the above-described methods, there is now need in new technologies that would make it possible to tailor the characteristics of films such as thickness, phase composition, and microstructure.

Technologies of thin-film materials based on yttrium iron garnet are yet developed insufficiently; there is great need in new strategies for design of items having tailored parameters. One rapidly developing strategy for forming 2D nanomaterials is sol—gel technology, where the precursors are hydrolytically active heteroligand complexes $[M(C_5H_7O_2)_x(OR)_y]$ prepared via controlled partial destructive substitution of alkoxy moieties for β-diketonate ligands. An alteration of composition in the coordination sphere of the precursor determines its reactivity and, accordingly, the kinetics of evolution of rheology in its solutions upon hydrolysis and polycondensation, which is of special importance for thin film formation. This strategy makes it possible to prepare both highly disperse metal oxides in powders [11–13], thin nanostructured films [14, 15], microtubes [16], or composite matrices [17] and refractory carbides [18–20].

Therefore, our study was focused on the specifics of synthesis of hydrolytically active heteroligand complexes $[M(C_5H_7O_2)_{3-x}(C_5H_{11}O^i)_x]$ ($M = Fe^{3+}$ and Y^{3+}) and the use of them in the manufacture of thin nanostructured films of yttrium iron garnet ($Y_3Fe_5O_{12}$) on sapphire substrates.

EXPERIMENTAL

Metal acetylacetonates were prepared from $Y(NO_3)_3 \cdot 6H_2O$ (chemically pure grade), $FeCl_3 \cdot 6H_2O$ (pure grade), $C_5H_8O_2$ (pure grade), and 5% aqueous solution of $NH_3 \cdot H_2O$ (high purity grade). The solvent used for the prepared chelates and the source of alkoxy groups in the synthesis of heteroligand complexes was isoamyl alcohol $^iC_5H_{11}OH$ (pure for analysis grade).

The precursors $[M(C_5H_7O_2)_{3-x}(C_5H_{11}O^i)_x]$ ($M = Fe^{3+}$ and Y^{3+}) were prepared by the heat treatment of a solution of iron and yttrium acetylacetonates in isoamyl alcohol inside a round-bottomed flask equipped with a refluxer on a sand bath.

Films of solution of heteroligand complexes were applied to polished polycrystalline sapphire substrates by the dip-coating method.

Electronic (UV–Vis) spectra of solutions of coordination compounds were recorded, before and after $C_5H_7O_2$ ligands were substituted, on an SF-56 UV–Vis spectrophotometer once the solutions were diluted with butanol (to $c = 4 \times 10^{-4}$ mol/L.

IR transmission spectra of solutions were recorded, before and after $C_5H_7O_2$ ligands were substituted, on an FT-08 Infralum FT-IR spectrometer (KBr glasses; wavenumber window: 350–4000 cm^{-1}).

The evolution of rheology of the solution of heteroligand precursor during hydrolysis and polycondensation was studied with a Fungilab Smart L rotational viscometer (shear speed: 100 rpm; L2 spindle; temperature: 22 ± 2°C).

X-ray diffraction patterns from the surfaces of oxide films were recorded on a D8 Advance (Bruker) X-ray diffractometer in the range of 2θ angles from 26° to 35° with 0.02° resolution and a signal accumulation time per point of 2 s.

The microstructure of oxide films was studied with an NVision 40 (Carl Zeiss) three-beam workstation equipped with an EDX Oxford Instruments energy-dispersive analysis unit, and with a Solver Pro-M scanning probe microscope (NT-MDT).

The adhesion of films was studied by a standard V-notch test using an Elcometer 107 adhesion meter.

RESULTS AND DISCUSSION

Synthesis of Heteroligand Precursors

A solution of the as-synthesized complexes $[Y(C_5H_7O_2)_3$ and $[Fe(C_5H_7O_2)_3]$ in isoamyl alcohol with the metal ratio set by the stoichiometry of the target oxide $Y_3Fe_5O_{12}$, was prepared in a round-bottomed flask equipped with a refluxer. The solution was heat treated at the boiling temperature (131 ± 2°C) on a sand bath for 4 h (the total metal concentration was 0.2 mol/L).

As a result, partial destructive substitution of $C_5H_{11}O^i$ groups for $C_5H_7O_2$ ligands occurred, which was verified by a reduction in intensity of IR absorption bands of the solution in the range 1500—1700 cm^{-1} (these bands relate to the stretching vibrations of C=C and C=O in coordinated chelate moieties) and the appearance of a new double absorption band in the range 1700–1760 cm^{-1} (this band arises from the ν(C=O) mode of reaction byproducts, namely acetone and ester).

In the UV–Vis spectrum of the solution of heteroligand precursors diluted to a metal concentration of 4×10^{-4} mol/L, the absorption band in the range 280–360 nm was also reduced in intensity (this range is characteristic of coordinated acetylacetonate ligands). The degree of substitution of alkoxy moieties for $C_5H_7O_2$ groups was 84% as estimated from the Bouguer–Lambert–Beer law.

How the rheology of the solution of heteroligand precursors changed upon hydrolysis and polycondensation was studied by rotational viscometry. Addition of a hydrolyzing component (ethanolic solution of water: 0.42 mL, $\varphi(H_2O) = 0.3$) to the $[M(C_5H_7O_2)_{3-x}(C_5H_{11}O)_x]$ (14 mL) solution induced hydrolysis and subsequent polycondensation, with an attendant increase in dynamic viscosity over time and the formation of a transparent gel (Fig. 1). Figure 1 makes it clear that the dynamic viscosity of the system increased by a factor of more than 10 (up to 210 cP) in 12 min, followed by a decrease to 130 cP (in 65 min after hydrolysis was initiated). The derivative curve (Fig. 1b) clearly shows the multistep character of the process. The maximal gel formation rate was attained on the sixth minute and amounted to about 35 cP/min to then decrease to a minimal value (of about –4 cP/min) in 8 min, followed by some increase and subsequent stabilization at a level of –1.5 cP/min manifested as a linear decline of the dynamic viscosity of the gel. Thus, we showed that the synthesized heteroligand precursors actively reacted with water with an attendant strong alteration of the rheology of their solutions, and this should be kept in mind in the manufacture of thin films of tailored thickness and tailored microstructure.

Application of Thin Films of Precursor Solutions to Polished Sapphire Substrates

As we showed earlier [15], when a thin film of a solution of $[M(C_5H_7O_2)_{3-x}(C_5H_{11}O)_x]$ precursors is applied to the substrate surface at 22°C, acetone and ester are consecutively evaporated from the film bulk (in 5 min), followed by the evaporation of isoamyl alcohol solvent (in 30 min). The hydrolysis of the heteroligand complexes by atmospheric moisture ends in 60 min. Relying on these results, we coated the surface of polished polycrystalline sapphire substrates with a thin film of the as-prepared solution of iron and yttrium alkoxyacetylacetonates by dip coating (withdrawal rate was 1 mm/s); afterwards, the samples were kept under air for 60 min to complete the formation of a thin xerogel film.

Crystallization of $Y_3Fe_5O_{12}$ Thin Films

The sapphire substrate samples coated with thin xerogel films were then heat-treated under various conditions in order to study the crystallization of yttrium iron garnet. Heating was performed to 800, 1000, and 1200°C at a rate of ~20 K/min under air without exposure and was followed by cooling.

The results of X-ray powder diffraction analysis of the surface of samples (Fig. 2) imply that the oxide film remains X-ray amorphous at 800°C. Heating of the xerogel coating to 1000°C resulted in the crystallization of the target cubic phase (yttrium iron garnet) with an average crystallite size of ~28 nm. When tem-

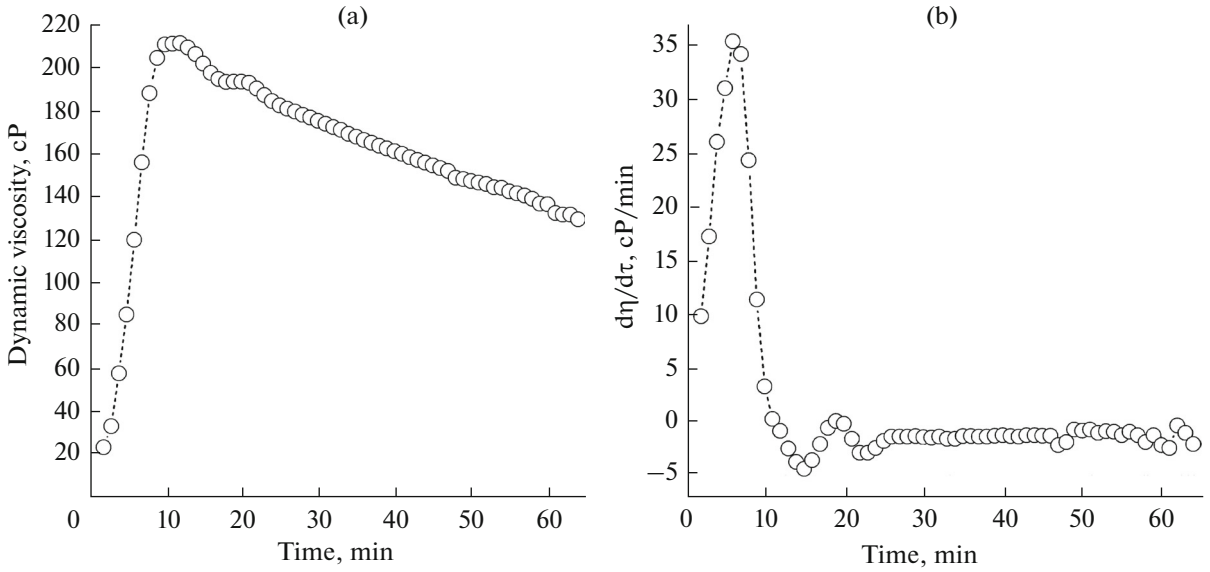

Fig. 1. (a) Dynamic viscosity of solution of iron and yttrium alkoxyacetylacetonates during hydrolysis and (b) its derivative curve.

perature increased further to 1200°C, the reflections from the garnet phase shifted toward greater angles, likely because of a partial interaction with the Al_2O_3 substrate and the formation of an oxide film of composition $Y_3Fe_{5-x}Al_xO_{12}$.

From the results of microstructure analysis by scanning electron microscopy (SEM), we may infer that the coating formed at 800°C was porous with a bimodal pore size distribution (with peaks at ~30 and ~150 nm) (Fig. 3). The microstructure retained this character upon heating to 1000°C, but the average pore size increased to ~40 and ~350 nm. Heating of the xerogel film to 1200°C gave a denser coating, which consisted of faceted particles having an average size of ~150 nm. An inspection of microdefects (Figs. 3g–3i) shows that the oxide films had thicknesses of ~150 nm, and an excessive thickness of the precursor solution layer (>200 nm) can give rise to the exfoliation of the coatings because of locally uncompensated surface tension at the syneresis stage of the gel film.

The energy dispersive elemental analysis of surface microregions of the films verified the set metal ratio and the formation of the oxide of composition $Y_3Fe_5O_{12}$.

The results of scanning probe microscopy (SPM) support the character of film microstructure derived from SEM images. The average size of constituent particles of the coating increased from 70 to 120 nm as temperature increased from 800 to 1000°C; the maximal height difference across the 25 μm^2 surface area increased from 30 to 50 nm (Fig. 4). For the yttrium iron garnet prepared at 1200°C, the height difference was ~70 nm.

The adhesion of oxide films was evaluated by a standard V-notch test. The nanostructured $Y_3Fe_5O_{12}$ coatings were found to refer to the maximal adhesion classes of the ISO (0) and ASTM (5B) international standards, and the coating technology may be recommended to the manufacturers of relevant structures.

In summary, we have studied the synthesis specifics of hydrolytically active heteroligand coordination

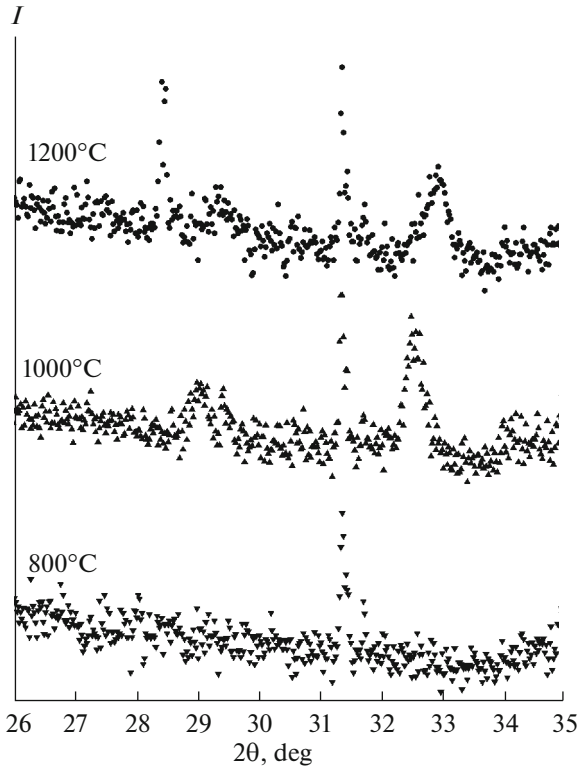

Fig. 2. X-ray diffraction patterns of $Y_3Fe_5O_{12}$ films prepared at various temperatures.

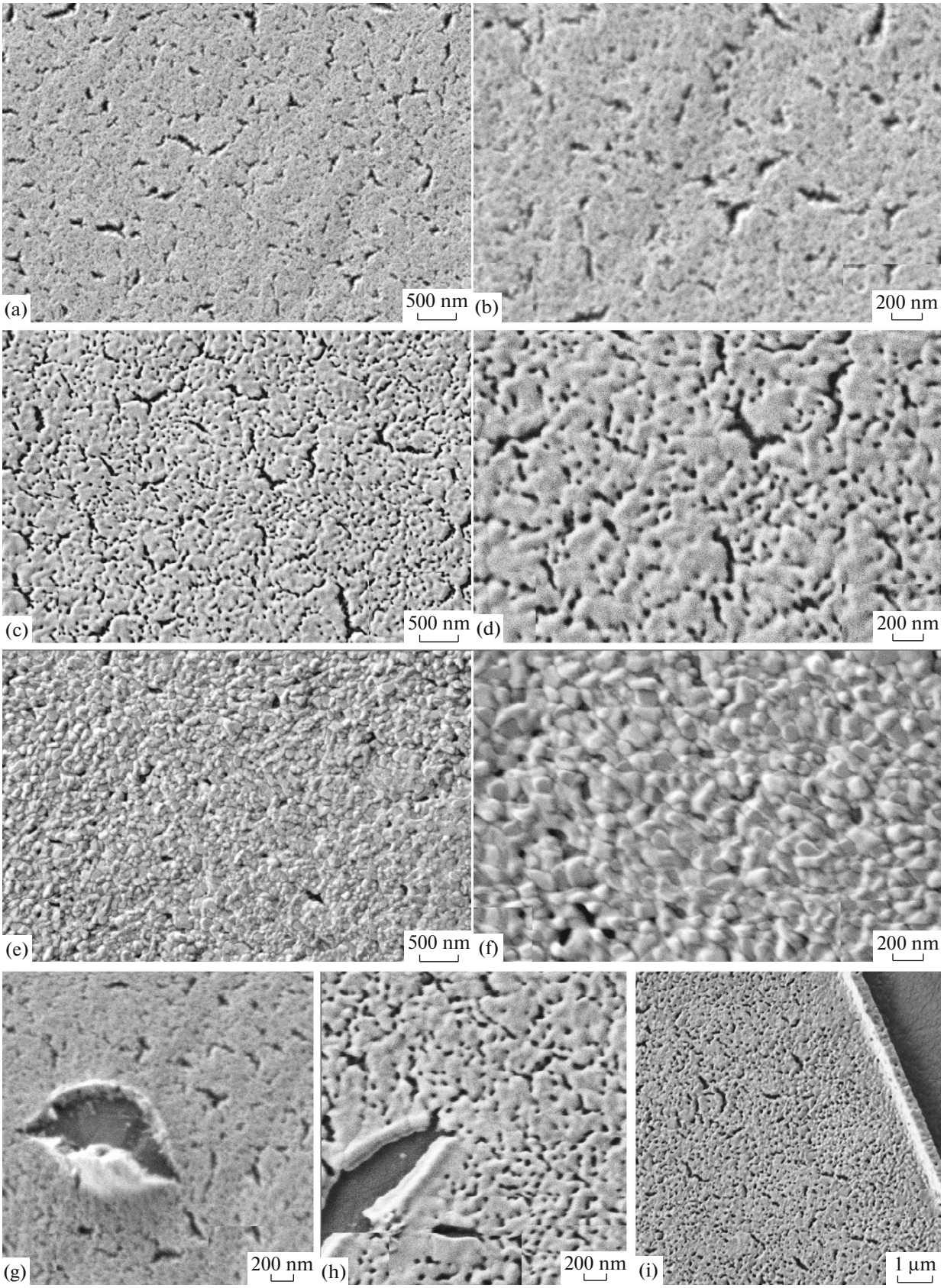

Fig. 3. Microstructure of $Y_3Fe_5O_{12}$ films prepared at (a, b) 800, (c, d) 1000, and (e, f) 1200°C, and (g, h, i) microdefects in the form of local exfoliations and breaks of films at (g) 800, (h) 1000, and (i) 1200°C (SEM).

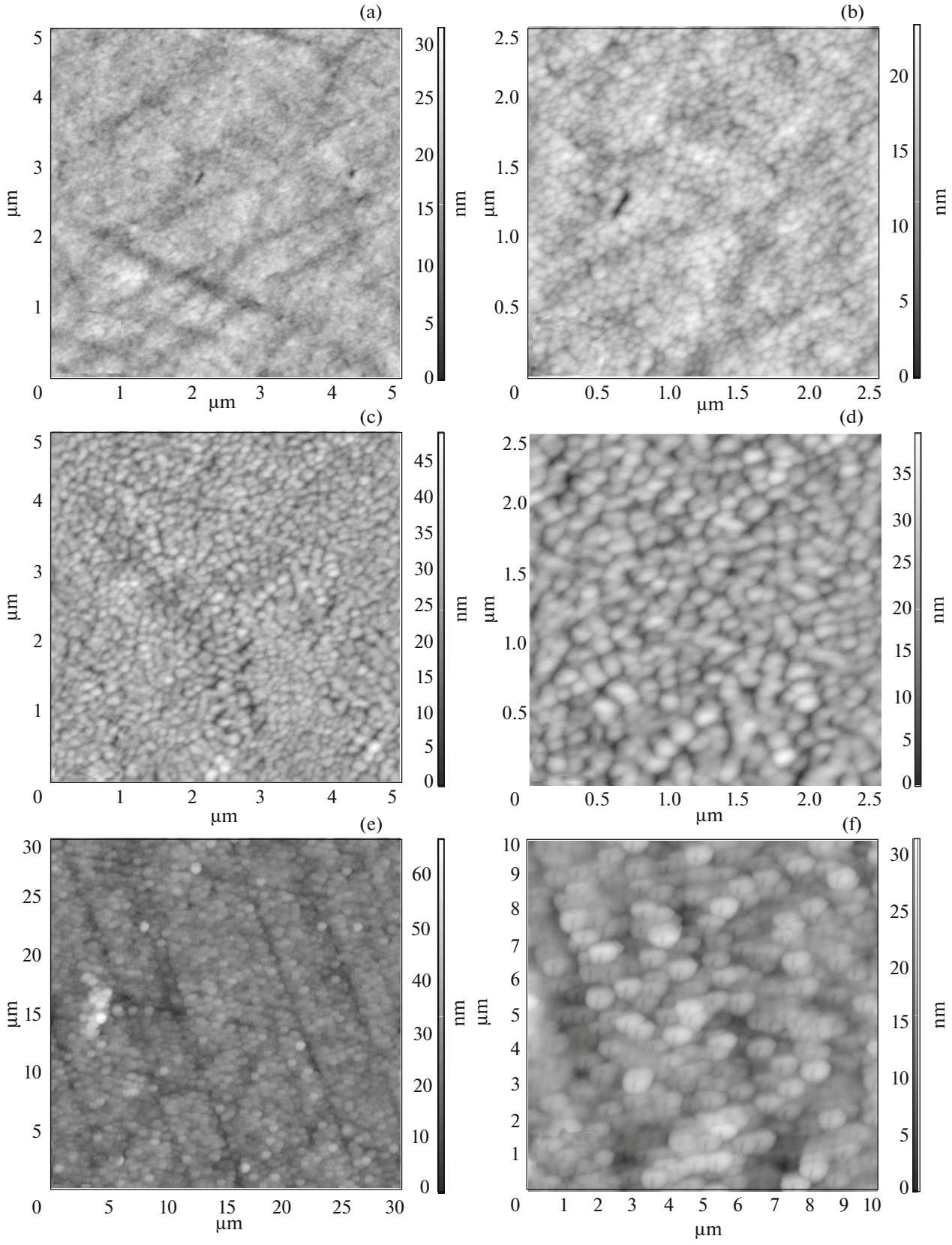

Fig. 4. Microstructure $Y_3Fe_5O_{12}$ films prepared at (a, b) 800, (c, d) 1000, and (e, f) 1200°C (SPM).

compounds $[M(C_5H_7O_2)_{3-x}(C_5H_{11}O^i)_x]$ ($M = Fe^{3+}$ and Y^{3+}) with a 84% degree of substitution of alkoxy moieties for chelating ligands, and studied the gel-formation kinetics of their solutions upon hydrolysis and polycondensation. We have used the precursor solutions to apply nanostructured thin films of yttrium iron garnet to sapphire substrates using dip coating technology to obtain an average crystallite size of ~28 nm. A nanostructured $Y_3Fe_5O_{12}$ coating has been found to crystallize when the xerogel film is heated above 800°C.

Scanning probe microscopy helped us to discover that the roughness of $Y_3Fe_5O_{12}$ films increases, as the synthesis temperature rises, from 30 (800°C) to 70 nm (1200°C); the films have the maximal adhesion classes according to international standards: ISO (0) and ASTM (5B).

ACKNOWLEDGMENTS

This study was supported by the Russian Foundation for Basic Research (project nos. 14-03-00983 A, 15-03-07568 A, 14-03-31002 mol_a, 15-29-01213 ofi_m, and 15-03-07568) and by a grant from the President of the Russian Federation (grant no. MK-4140.2015.3).

REFERENCES

1. T. Boudiar, B. Payet-Gervy, M.-F. Blanc-Mignon, et al., J. Magn. Magn. Mater. **284**, 77 (2004).
2. M.-B. Park and N.-H. Cho, J. Magn. Magn. Mater. **231**, 253 (2001).
3. S. A. Manuilov, R. Fors, S. I. Khartsev, et al., J. Appl. Phys. **105**, 033917 (2009).
4. N. B. Ibrahim, C. Edwards, and S. B. Palmer, J. Magn. Magn. Mater. **220**, 183 (2000).
5. Y. Nakata, T. Okada, M. Maeda, et al., Opt. Lasers Eng. **44**, 147 (2006).
6. X. Zhou, W. Cheng, F. Lin, et al., Appl. Surf. Sci. **253**, 2108 (2006).
7. N. Kumar, D. S. Misra, N. Venkataramani, et al., J. Magn. Magn. Mater. **272—276**, E899 (2004).
8. G. Siegel, M. C. Prestgard, S. Teng, et al., Sci. Rep. **4**, 4429/1 (2014).
9. M. Nur-E-Alam, M. Vasiliev, K. Alameh, et al., J. Nanomater. **2015**, 1 (2015).
10. O. Galstyan, H. Lee, A. Babajanyan, et al., J. Appl. Phys. **117**, 163914 (2015).
11. N. T. Kuznetsov, V. G. Sevast'yanov, E. P. Simonenko, et al., RU Patent 2407705 (2010).
12. V. G. Sevast'yanov, E. P. Simonenko, N. P. Simonenko, et al., Russ. J. Inorg. Chem. **57**, 307 (2012). doi 10.1134/S0036023612030278
13. E. P. Simonenko, N. P. Simonenko, V. G. Sevastyanov, et al., Russ. J. Inorg. Chem. **57**, 1521 (2012). doi 10.1134/S0036023612120194
14. N. T. Kuznetsov, V. G. Sevast'yanov, E. P. Simonenko, et al., RU Pat. 2521643 (2014)
15. N. P. Simonenko, E. P. Simonenko, V. G. Sevastyanov, et al., Russ. J. Inorg. Chem. **60**, 795 (2015). doi 10.1134/S0036023615070153
16. N. P. Simonenko, E. P. Simonenko, V. G. Sevast'yanov, et al., Yad. Fiz. Inzh. **5**, 331 (2014).
17. E. P. Simonenko, N. P. Simonenko, V. G. Sevastyanov, et al., Compos. Nanostruct., No. 4, 52 (2011).
18. V. G. Sevastyanov, E. P. Simonenko, N. A. Ignatov, et al., Russ. J. Inorg. Chem. **56**, 661 (2011). doi 10.1134/S0036023611050214
19. E. P. Simonenko, N. A. Ignatov, N. P. Simonenko, et al., **56**, 1681 (2011). doi 10.1134/S0036023611110258
20. N. T. Kuznetsov, V. G. Sevastyanov, E. P. Simonenko, et al., RU Pat. No. 2333888 (2008).

Translated by O. Fedorova